IEEE Access
The journal for rapid open access publishing

IEEE Xplore Digital Library
http://ieeexplore.ieee.org/Xplore

An Efficient Radio Resource Allocation Scheme in Dynamic Ultra-Dense Heterogeneous Networks

Chongyu Niu†, Yibing Li†, Rose Qingyang Hu‡, Fang Ye†
†Department of Information and Communication Engineering, Harbin Engineering University, Harbin, Heilongjiang, China
‡Department of Electrical and Computer Engineering, Utah State University,Logan,UT,USA
Email: †{niuchongyu@hrbeu.edu.cn, liyibing@hrbeu.edu.cn, yefang@hrbeu.edu.cn}, ‡rosehu@ieee.org

***Abstract*—Ultra-dense network (UDN) is considered as a promising technology in 5G wireless networks. In an UDN network, dynamic traffic load distribution can lead to a high computational pressure and a high communications overhead on traditional universal sub-band reuse schemes. In this paper, a low computational overhead and a low sub-band hand-off rate resource allocation scheme in an dynamic ultra-dense Heterogeneous Network(UDHN) is presented. The scheme first defines a new interference estimation method that constructs network interference state map, based on which a radio resource allocation scheme is proposed. The resource allocation problem is a MAX-K cut problem and solved via a graph-theoretical approach. System level simulations reveal that with the proposed scheme the sub-band hand-off decreases by 30% with less than 3.2% network throughput degradation.**

***Index Terms*—LTE-A HetNets, graph theory, femtocell, MAX-K cut**

I. Introduction

The demand for ubiquitous availability of reliable and high data rate mobile services is exploding. The mobile data traffic demand has been predicted to have a 1000-fold increase in the next 20 years [1], [2]. To meet the explosive capacity increase of mobile communication systems, Ultra-dense Networking (UDN) has been widely considered as a promising technology [3]. In addition, studies predict that more than 50% of voice calls and more than 70% of data traffic in the future wireless networks originated from indoors [4]. Thus, femtocells (FCs) that are mainly deployed indoors will play a significant role in the 5G network access, especially for low velocity or stationary users [5]. Ultra-dense deployed FCs overlaid with traditional macrocells (MCs) leads to a more complex network, namely, Ultra-Dense Heterogeneous Network (UDHN).

With the explosive growth of mobile devices capacity and cloud computing, the latency of the communication, reliability of the services, and pervasive availability of the networks are among the most important performance metrics when deploying 5G UDHNs. According to the METIS project, there are mainly five features of 5G communication systems: 1) amazingly fast, 2) great service in a crowd, 3) ubiquitous things communicating, 4) best experience follows you, and 5) super real-time and reliable connections [6]. In UDHNs, there are a number of technical challenges [7], among which one of the most important challenges is how to efficiently allocate and utilize sub-band resources to improve the spectrum efficiency and mitigate interference. Furthermore, in a dynamic UDHN, sub-band resource allocation should be rather stable and any sub-band hand-off should be swift.

There have been extensive ongoing research on sub-band resource allocation [8]–[10], which are mainly classified into centralized approaches and decentralized approaches. However, most of the existing schemes used in the traditional heterogeneous networks(HetNets) will not be suitable in the UDHN. There are two reasons: i) Existing decentralized approaches will need a long time to get convergence due to the huge amount of nodes in the UDHN, which will not meet the super real-time and reliable requirement of UDHN; ii) The traditional centralized approach can achieve optimal/near-optimal resource allocation performance, while the huge computational overhead makes this approach impractical. Especially in the dynamic UDHN, the rapidly changed network state will lead to an unacceptable computational pressure to the traditional resource allocation schemes. So, an efficient resource allocation scheme that providing rapid and stable resource allocation decisions for dynamic UDHN is urgently needed to be addressed.

Lately a lot of work have been done concentrating on the dynamic interference mitigation problem in UDHNs. In [11]–[17], the authors try to solve the resource allocation problem in the clustering based graph scheme. In [11], the effect of clustering based resource allocation scheme has been investigated in a femtocell dense deployed network. In this paper, the resource allocation problem is formulated as a mixed integer non-linear program, and the proposed scheme can achieve near optimal performance in interference mitigation with a reduced computational complexity. In [12], the authors jointly consider the real time interference and traffic characteristics of the heavily overlapped femtocells based on the clustering scheme. In [13], a suboptimal sub-band assignment and interference management algorithm is designed based on an adaptive graph coloring approach and fractional frequency reuse scheme. All of [11] [12] and [13] can achieve a good performance in co-tier interference or cross-tier interfer-

Digital Object Identifier: 10.1109/ACCESS.2017.2653798

ence controlling, but in the dynamic network condition in UDHN they do not work well. In [14]–[17], the dynamic network condition has been studied. In [14], the dynamic interference coordination problem has been studied in a dynamic graph based scheme. In this scheme, a two tier clustering scheme is used to divide the femtocells and UEs into several small groups. This scheme can achieve more than 90% of the optimal performance, while the huge communication overhead is not considered. In [15], a multi-cluster based dynamic sub-band assignment method is discussed in UDNs. The scheme divides the entire spectrum into two groups, namely dynamic group and static group. Different types of UEs will be assigned different kind of sub-bands. In this scheme the static UEs can get a stable transmit experience, but the partition of the spectrum actually lowers down the spectral efficiency. Further, the computational complexity is not considered in this paper. In [16], the authors propose an interference weight calculaition algorithm to reduce the computational complexity in the dynamic cell clustering scheme. The computational complexity can be reduced to half compared to the traditional clustering based scheme, but the feasibility of this algorithm in dynamic UDHN is not discussed. In [17], an interference-separation clustering based scheme is used to lower down the huge communication overhead and computational complexity in the dynamic UDHN. In this scheme, massive small cells are divided into different small groups with different priorities to reduce the complexity. This scheme can achieve a well real time resource allocation, while the spectral efficiency can be low due to the unclear interference weight calculation.

In all the above papers, sub-band hand-off between different sub-band allocation time slots has been ignored. Unnecessary sub-band hand-off leads to a high latency and low reliability of the services. To tackle this problem, in this paper a new fast sub-band allocation scheme with low sub-band hand-off rate is proposed based on the graph clustering theory. Different from the traditional clustering schemes, in which only part of the sub-bands are made accessible to FCs, a more flexible UFR approach is used to offer a higher spectral efficiency. The proposed scheme first presents the system model and proposes a potential interference estimation method between different users in HetNets, including intra-tier and inter-tier interference estimation. A network Interference State Map (ISM) is constructed to compare the network state information between different sub-band allocation time slots (TSs). Afterwards, a cluster-based sub-band allocation algorithm in a universal spectrum reuse scheme is discussed and a fast sub-band allocation scheme (FAS) based on the ISM and sub-band allocation algorithm is presented.

The main contributions of this paper are summarized in the following. 1) A new fast sub-band allocation scheme with low sub-band hand-off rate is developed. 2) A new interference evaluation model in the two-tier ultra-dense deployed heterogeneous networks is defined. 3) A new ISM model is proposed to describe the complex HetNets interference situation.

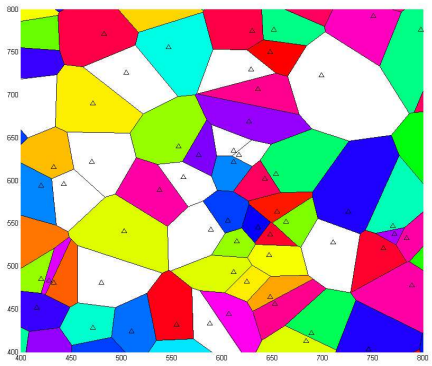

Figure 1. The Voronoi Femtocell Topology (Δ stands for an FBS)

The remainder of this paper is organized as follows. The system model is shown in Section II. In Section III, the fast sub-band allocation scheme is elaborated. Section IV evaluates the performance of the proposed scheme via simulations. Section V draws the conclusion of the paper.

II. System model and problem formulation

A. System Model

In a two-tier UHDN, one MBS with a coverage radius R_M is located at the center and a number of FBSs are densely deployed within the coverage of that MBS. Two different UEs are considered, namely MUEs served by the MBS and FUEs served by FBSs. Both MUEs and FUEs are distributed randomly with respective densities as λ_m and λ_f [18]. FBSs constitute the femto-tier and the coverage area of each FBS is a circular region with a radius of R_f. In an UDHN, different FBSs can have overlapped coverage areas due to the high density of FBSs. So the actual service area of FBSs induces a Voronoi tessellation [19], as shown in Fig.1.

In each time slot, $n_{(m,t)}$ MUEs and $n_{(f,t)}$ FUEs can join, leave or change their locations in the network. Each cell, either an MC or a FC, constitutes an independent agent that performs autonomous radio resource allocation decisions with the objective of improving signal to interference plus noise ratio (SINR) while guaranteeing quality of service (QoS). All the system configuration information is accessible at the MBS. These information can include geographic locations of MUEs, FBSs and FUEs, the channel fading parameters, and dynamic system information.

As shown in the green marked part in Fig. 2, wireless links and their respective received powers in this UHDN can be classified into five types [20]:

(1) Outdoor link from MBS to MUE m

$$P_m^{k,t} = P_{B,m}^{k,t} h_{B,m}^{k,t} G_{B,m}^{k,t}. \quad (1)$$

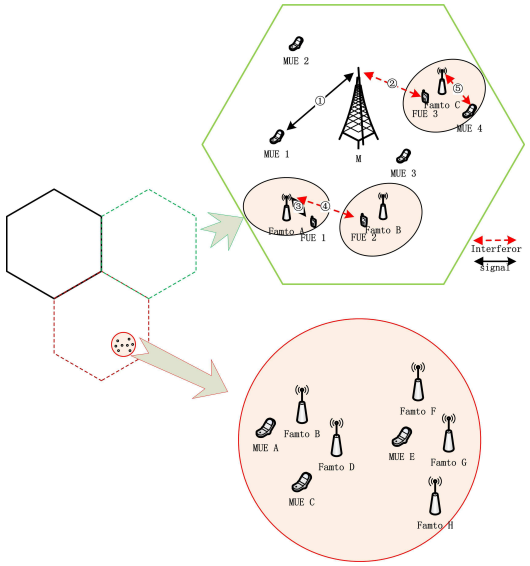

Figure 2. Proposed Dense Framework for Sub-band Assignment

(2) Outdoor-to-Indoor link from MBS to FUE j_f

$$I_{B,j_f}^{k,t} = \sum_{m \in \boldsymbol{M}} s_m^{k,t} P_{B,m}^{k,t} h_{B,j_f}^{k,t} G_{B,j_f}^{k,t}. \quad (2)$$

(3) Indoor link from FBS f to its serving FUE j_f

$$P_{j_f}^{k,t} = P_{f,j_f}^{k,t} h_{f,j_f}^{k,t} G_{f,j_f}^{k,t}. \quad (3)$$

(4) Indoor-to-indoor link from FBSs in the different FCs to FUE j_f

$$I_{\boldsymbol{F^*},j_f}^{k,t} = \sum_{f^* \in \boldsymbol{F^*}} \sum_{j_{f^*} \in \boldsymbol{J_{f^*}}} s_{j_{f^*}}^{k,t} P_{f^*,j_{f^*}}^{k,t} h_{f^*,j_f}^{k,t} G_{f^*,j_f}^{k,t}. \quad (4)$$

(5) Indoor-to-Outdoor link from FBS to MUE m

$$I_{\boldsymbol{F},m}^{k,t} = \sum_{f \in \boldsymbol{F}} \sum_{j_f \in \boldsymbol{J_f}} s_{j_f}^{k,t} P_{f,j_f}^{k,t} h_{f,m}^{k,t} G_{f,m}^{k,t}. \quad (5)$$

$\boldsymbol{K} = \{k|k = 1,2,...,K\}$ stands for the set of total sub-bands; $\boldsymbol{M} = \{m|m = 1,2,...,M\}$ stands for the set of MUEs located in the coverage area of the MBS; $\boldsymbol{F} = \{f|f = 1,2,...,F\}$ stands for the set of FBSs located in the coverage of MBS; $\boldsymbol{F^*} : \{f^* \in \boldsymbol{F^*}\}$ stands for the set of FBSs located in the coverage of MBS but exluding FBS f; $\boldsymbol{J_f} : \{j_f \in \boldsymbol{J_f}\}$ stands for the set of FUEs served by FBS f; $\boldsymbol{J_F} : \{\boldsymbol{J_f} \in \boldsymbol{J_F}\}$ stands for the set of FUEs in the coverage of the MBS; B stands for the MBS; $P_{B,m}^{k,t}$ ($P_{f,j_f}^{k,t}$) stands for the transmit power from MBS (FBS f) to MUE m (FUE j_f) on sub-band k in time slot t; $h_{B,m}^{k,t}$ ($h_{f,j_f}^{k,t}$) denotes the channel gain from MBS (FBS f) to MUE m (FUE j_f) on sub-band k in time slot $t$and follows an exponential distribution; $G_{B,m}^{k,t}$ ($G_{f,j_f}^{k,t}$) denotes the path loss from MBS (FBS f) to MUE m (FUE j_f) on sub-band k in time slot t. $s_m^{k,t}$ is the sub-band allocation indicator, i.e., $s_m^{k,t} = 1$ if sub-band k is assigned to UE m in time slot t , while $s_m^{k,t} = 0$ otherwise. We assume the same K channels are used in all the cells, including one MBS and N_F FBSs.

$SINR_m^{k,t}$ represents the SINR for downlink transmission from MBS to MUE m on sub-band k in time slot t and is expressed as:

$$SINR_m^{k,t} = \frac{P_m^{k,t}}{I_{\boldsymbol{F},m}^{k,t} + N_0}. \quad (6)$$

The SINR for downlink transmission from FBS f to FUE j_f on sub-band k in time slot t is given by:

$$SINR_{j_f}^{k,t} = \frac{P_{j_f}^{k,t}}{I_{B,j_f}^{k,t} + I_{\boldsymbol{F^*},j_f}^{k,t} + N_0}, \quad (7)$$

$I_{\boldsymbol{F},m}^{k,t}$ represents the interference from all co-channel FBSs to MBS on channel k in time slot t; $I_{B,j_f}^{k,t}$ represents co-channel interference from MBS to FBS j_f on channel k in time slot t; $I_{\boldsymbol{F^*},j_f}^{k,t}$ represents co-channel interference from all other FBSs to FBS j_f on channel k in time slot t; N_0 stands for the noise level.

B. Problem Formulation

All the FUEs in the serving area of an FBS share the resources assigned to that FBS orthogonally. Without loss of generality, It is assumed that the radio resources are allocated in the unit of sub-band and each user is assigned an equal number of subbands, which is set to one sub-band without loss of generality. The FAS scheme aims to construct a fast sub-band allocation while minimize unnecessary sub-band switch among users. Users that stay in the same condition (including location, activation state) in two different time slots are defined as static users (U^S), which inlcude static macro users (U_M^S) and static femto users (U_F^S). Also, users that join, leave or change their locations in two different time slots are defined as dynamic users (U^D), including dynamic macro user (U_M^D) and dynamic femto user (U_F^D). In consideration of the energy saving, FBSs serving no FUE are turned off, shown as white colored areas in Fig.1. Only FBSs with active FUEs in their Voronoi serving areas are allocated sub-bands. So the total number and the locations of FBSs keep the same but the number of active FBSs may change from time to time.

In two different time slots, the network interference topology could be different. Fig. 3 I is the network interference topology of red marked area shown in Fig. 2, where circles stand for UEs, solid lines between different circles stand for co-channel interference when two users use the same sub-band, and different colors stand for different sub-band. So the corresponding interference matrix can be expressed as:

$$I_I = \begin{bmatrix} i_{AA} & i_{AB} & \cdots & i_{AH} \\ i_{BA} & \ddots & & \vdots \\ \vdots & & \ddots & \vdots \\ i_{HA} & \cdots & \cdots & i_{HH} \end{bmatrix}$$
$$= \begin{bmatrix} 1 & 1 & 1 & 0 & 0 & 0 & 0 & 0 \\ 1 & 1 & 1 & 1 & 0 & 0 & 0 & 0 \\ 1 & 1 & 1 & 1 & 0 & 0 & 0 & 0 \\ 0 & 1 & 1 & 1 & 1 & 0 & 0 & 0 \\ 0 & 0 & 0 & 1 & 1 & 1 & 1 & 1 \\ 0 & 0 & 0 & 0 & 1 & 1 & 1 & 0 \\ 0 & 0 & 0 & 0 & 1 & 1 & 1 & 1 \\ 0 & 0 & 0 & 0 & 1 & 0 & 1 & 1 \end{bmatrix}. \quad (8)$$

Due to the user's movement, the network interference topology may become Fig. 3 II and Fig. 3 III after certain time. The corresponding interference matrix of II is:

$$I_{II} = \begin{bmatrix} 1 & 1 & 1 & 0 & 0 & 0 & 0 & 0 \\ 1 & 1 & 1 & 1 & 0 & 0 & 0 & 0 \\ 1 & 1 & 1 & 0 & 0 & 0 & 0 & 0 \\ 0 & 1 & 0 & 1 & 1 & 0 & 0 & 0 \\ 0 & 0 & 0 & 1 & 1 & 1 & 1 & 1 \\ 0 & 0 & 0 & 0 & 1 & 1 & 0 & 0 \\ 0 & 0 & 0 & 0 & 1 & 0 & 1 & 1 \\ 0 & 0 & 0 & 0 & 1 & 0 & 1 & 1 \end{bmatrix}. \quad (9)$$

Comparing interference matrices (8) and (9), one can see that even though users A, C, D, and G have changed their locations, the interference relationship between different users still keep quite the same. Thus there is no need to change the original sub-band allocations among users. In another different scenario, as shown in Fig. 3 III, even though only users D and E change their locations, the entire network interference relationship changes and the corresponding interference matrix of III becomes:

$$I_{III} = \begin{bmatrix} 1 & 1 & 1 & 0 & 0 & 0 & 0 & 0 \\ 1 & 1 & 1 & 0 & 1 & 0 & 0 & 0 \\ 1 & 1 & 1 & 1 & 1 & 0 & 0 & 0 \\ 0 & 0 & 1 & 1 & 1 & 0 & 0 & 1 \\ 0 & 1 & 1 & 1 & 1 & 1 & 1 & 1 \\ 0 & 0 & 0 & 0 & 1 & 1 & 1 & 0 \\ 0 & 0 & 0 & 0 & 1 & 1 & 1 & 1 \\ 0 & 0 & 0 & 1 & 1 & 0 & 1 & 1 \end{bmatrix}. \quad (10)$$

From matrices (8) and (10), the network sub-band allocation needs to be updated and we call this update as subband switch. The condition that triggers sub-band switch is critical in the FAS scheme.

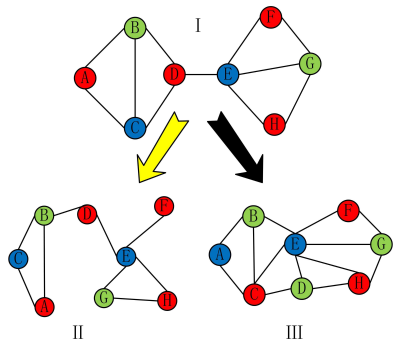

Figure 3. Network Interference Topology Variation Due to UE mobility

We define the sub-band switch indicator(SSI) to represent the sub-band switch, i.e. $SSI_u^t = 0$, subject to:

$$\begin{cases} s_u^{k,t} = s_u^{k',t-1}; \\ s_u^{k,t} = 1, \qquad \forall k, k' \in \boldsymbol{K}, u \in \boldsymbol{U}; \\ k = k'. \end{cases} \quad (11)$$

Otherwise, $SSI_u^t = 1$. Where, $s_u^{k,t}(s_u^{k',t-1})$ is the sub-band allocation indicator. $\boldsymbol{U} = \boldsymbol{M} \cup \boldsymbol{J_F}$ is the set of all UEs in the coverage area of MBS.

The objective of the proposed scheme is to minimize the sub-band hand-off frequency(SHF). So the optimization problem is formulated as:

$$\min(\frac{\sum_{t \in \boldsymbol{T}} SSI_u^t}{T}), \forall u \in \boldsymbol{U} \quad (12)$$

$\boldsymbol{T}$ is the total number of time slot in the whole test stage.

III. Proposed Solution

A. Interference Estimation

In the FAS scheme, the sub-band resource allocation can be decided based on the interference matrix. In UDHNs, network interference topology is much more complicated than what is shown in Fig.3. In [21] the Regional Average Channel Quality (RAQ) metric is used to estimate interference. RAQ of region A_i that is served by BS_i and is interfered by BS_j is expressed as $R_{(i,j,A_i)}$. It represents the average $SINR$ in A_i and can be calculated as:

$$\begin{aligned} & R_{(BS_i,BS_j,A_i)} \\ &= \iint_{A_i} SINR_{i,j}(x,y)dxdy \Big/ S(A_i) \\ &= \iint_{A_i} \frac{P_{r,i}(x,y)}{P_{r,j}(x,y) + N_0} dxdy \Big/ S(A_i), \end{aligned} \quad (13)$$

$\mathrm{SINR}_{i,j}(x,y) = P_{r,i}(x,y) / (P_{r,j}(x,y) + N_0)$; $P_{r,i}(P_{r,j})$ is the received power from BS_i (BS_j); N_0 is the noise power; $S(A_i)$ is the area size of region A_i.

To further evaluate the total potential influence one UE can make to the entire network when it uses a specific sub-band, Accumulate Regional Average Interference Strength (AAS) is further defined. We use the coverage area as the evaluating area of one FBS. The calculation method of AAS varies between MUE and FUE.

1) AAS Calculation for FUEs: In HetNets, an FUE can cause inter-tier interference to a co-channel MUE and intra-tier interference to co-channel FUEs in adjacent FBSs.

- AAS from Intra-tier Interference
  Assume FBS f is located at $(0,0)$ with a transmit power $P_f = \frac{P_{FBS}}{|\boldsymbol{J_f}|}$ and another FBS f^* is located at $(d,0)$ with a transmit power $P_{f^*} = \frac{P_{FBS}}{|\boldsymbol{J_{f^*}}|}$. When FUE j_f served by FBS f is located at (x,y), the signal powers this FUE receives from FBS f and f^* are respectively expressed as

$$P_{r,f} = P_f (x^2+y^2)^{-\frac{\alpha}{2}}. \tag{14}$$

$$P_{r,f^*} = P_{f^*}((x-d)^2+y^2)^{-\frac{\alpha}{2}}. \tag{15}$$

  RAQ for FUE j_f is then calculated as

$$\begin{aligned} &R_{(f,f^*,A_f)} \\ &= \iint\limits_{A_f} SINR_{f,f^*}(x,y)dxdy \Big/ S(A_f) \\ &= \iint\limits_{A_f} \frac{P_f (x^2+y^2)^{-\frac{\alpha}{2}}}{P_{f^*}((x-d)^2+y^2)^{-\frac{\alpha}{2}} + N_0} dxdy \Big/ S(A_f). \end{aligned}$$

  In the urban channel model, $\alpha = 2$ and noise is neglected. One can get RAQ for FUEj_f as

$$\begin{aligned} &R_{(f,f^*,A_f)} \\ &\approx \frac{P_f}{P_{f^*}} \iint\limits_{A_f} \frac{(x-d)^2+y^2}{x^2+y^2} dxdy \Big/ S(A_i) \\ &= \frac{P_f}{P_{f^*}} \left(1 + \frac{2d^2}{{R_f}^2 - {R_{min,f}}^2} \ln \frac{R_f}{R_{min,f}}\right) \\ &= \frac{P_f}{P_{f^*}} \left(1 + 2d^2 \psi_f\right), \\ &\psi_f = \frac{1}{{R_f}^2 - {R_{min,f}}^2} \ln \frac{R_f}{R_{min,f}}. \end{aligned} \tag{16}$$

  R_f stands for the coverage radius of FBS f; $R_{min,f}$ stands for the minimum distance between FBS f and its serving FUEs.
  In this paper, we assume that BSs in the same tier have the same transmit power, the same coverage radius and the same minimum UE to BS distance. Then AAS from FBS f to all other FBSs is:

$$\begin{aligned} &I^{AAS}_{(\boldsymbol{F^*},f,\boldsymbol{A_{F^*}})} \\ &= \sum_{f^* \in \boldsymbol{F^*}} \frac{1}{R_{f^*,f,A^*}} \\ &= \sum_{f^* \in \boldsymbol{F^*}} \frac{1}{1+2d^2_{f^*,f}\psi_{f^*}}. \end{aligned} \tag{17}$$

  $d_{f^*,f}$ is the distance between FBS $f*$ and FBS f.
- AAS from Inter-tier Interference
  Assume FBS f is located at $(0,0)$ with a transmit power P_f and MBS B is located at $(d,0)$ with a transmit power $P_B = \frac{P_{FBS}}{K}$. There are N_M MUEs distributed uniformly in the coverage of MBS. Each FBS only serves one FUE. When FUE j_f served by FBS f is located at (x,y), the signal power the FUE received from MBS is

$$P_{r,B} = P_B((x-d)^2+y^2)^{-\frac{\alpha}{2}}. \tag{18}$$

  So the RAQ for FUE f is:

$$R_{(f,B,A_f)} = \frac{P_f}{P_B}\left(1+2d^2\psi_f\right). \tag{19}$$

  The value of AAS that FBS f makes to all the MUEs is:

$$\begin{aligned} I^{AAS}_{(\boldsymbol{M},f)} &= \sum_{m \in \boldsymbol{M}} \frac{1}{SINR_m} \\ &= \sum_{m \in \boldsymbol{M}} \frac{1}{\frac{P_B ({d_{m,B}}^2)^{-1}}{P_f ({d_{m,f}}^2)^{-1}}} \\ &= \sum_{m \in \boldsymbol{M}} \frac{P_f {d_{m,B}}^2}{P_B {d_{m,f}}^2}. \end{aligned} \tag{20}$$

  $d_{m,B}$ stands for the distance between MUE m and MBS; $d_{m,f}$ stands for the distance between MUE m and FBS f.
  In summary, the AAS value of FUE f, including both intra-tier and inter-tier AAS, can be expressed as:

$$I^{AAS}_f = \sum_{f^* \in \boldsymbol{F^*}} \frac{1}{1+2d^2_{f^*,f}\psi_{f^*}} + \sum_{m \in \boldsymbol{M}} \frac{P_f {d_{m,B}}^2}{P_B {d_{m,f}}^2}. \tag{21}$$

2) AAS Calculation for MUEs: So when an MUE uses a specific sub-band, the AAS from MUE to other UEs is the AAS from MBS to all the other MUEs and FBSs in the coverage of this MBS. Here we also discuss these two interference scenarios separately.

- AAS for Intra-tier Interference

$$\begin{aligned} I^{AAS}_{(m^*,m)} &= \sum_{\substack{m^*,m \in \boldsymbol{M} \\ m^* \neq m}} \frac{1}{SINR_{m^*}} \\ &= \sum_{\substack{m^*,m \in \boldsymbol{M} \\ m^* \neq m}} \frac{1}{\frac{P_B d^{-\frac{\alpha}{2}}_{m^*,B}}{P_{m,B} d^{-\frac{\alpha}{2}}_{m^*,B} \lambda_{m^*,m}}}. \end{aligned} \tag{22}$$

In this paper, we assume the MBS average its transmit power in every sub-band. So

$$I^{AAS}_{(m^*,m)} = \sum_{\substack{m^*,m\in \boldsymbol{M} \\ m^*\neq m}} \lambda_{m^*,m}, \tag{23}$$

subject to:

$$\begin{cases} \lambda_{m^*,m} = 1, & \boldsymbol{\Theta_m} = \boldsymbol{\Theta_{m^*}}; \\ \boldsymbol{\varpi^{-1}}, & \boldsymbol{\Theta_m} \neq \boldsymbol{\Theta_{m^*}}. \end{cases} \tag{24}$$

$\boldsymbol{\varpi}$ stands for the antenna back loss; $\boldsymbol{\Theta_m}$ stands for the sector label of UE m.

- AAS for Inter-cell Interference
We consider the scenario that an MBS is located at $(0,0)$ with the transmit power P_B and an FBS is located at $(d,0)$ with the transmit power P_f. When the MUE m is located at (x,y), the signal power the MUE receives from the MBS is

$$P_{r,B} = P_B(x^2+y^2)^{-\frac{\alpha}{2}}. \tag{25}$$

The signal power MUE receive from FBS f is

$$P_{r,f} = P_f((x-d)^2+y^2)^{-\frac{\alpha}{2}}. \tag{26}$$

So the AAS for MUE m to all FBSs is expressed as

$$\begin{aligned} I_{(\boldsymbol{F},m,\boldsymbol{A_F})} &= \sum_{f\in\boldsymbol{F}} \frac{1}{R_{(f,m,A_f)}} \\ &= \sum_{f\in\boldsymbol{F}} \frac{P_B}{P_f\left(1+2d^2_{f,B}\psi_f\right)}. \end{aligned} \tag{27}$$

$d_{f,B}$ stands for the distance between FBS f and MBS. In summary, the AAS for MUE m, including both intra-tier and inter-tier AAS, can be expressed as:

$$I^{AAS}_m = \sum_{\substack{m^*,m\in\boldsymbol{M} \\ m^*\neq m}} \lambda_{m^*,m} + \sum_{f\in\boldsymbol{F}} \frac{P_B}{P_f\left(1+2d^2_{f,B}\psi_f\right)}. \tag{28}$$

B. Network Interference State Map (ISM)

In this part we discuss the network interference state map (ISM) construction process. The ISM covers an area of $2R_M * \sqrt{3}R_M$ with $\Psi * 0.866\Psi$ pixels, where the length of one pixel ψ is the minimum distance between two different users, $\Psi = \frac{2R_M}{\psi}$. The MBS locates at the center of ISM, with coordinate $(0,0)$. And the coverage area of the MBS is divided into three sectors, sector.0, sector.1 and sector.3. We set the value of the pixels located outside the hexagonal MBS coverage area as 0. The interference map includes two layers, MUE layer and FBS layerm which are discussed separately.

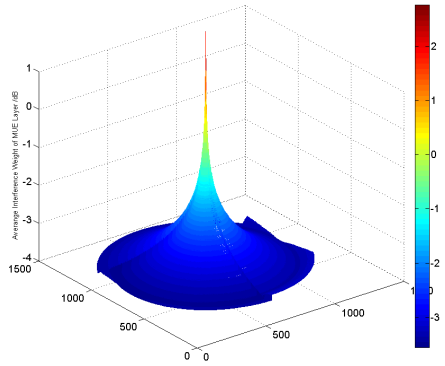

Figure 4. ISM for MUE Layer

1) Interference State Map Pixel Weight for MUE Layer: We first calculate the average interference weight $h_m(i,j)$ on ISM pixel with the coordinate $(i,\ j)$. Without loss of generality, we use sector.0 as an example:

$$I^{AAS}_{\boldsymbol{M}} = \sum_{m\in\boldsymbol{M_{S_0}}} I^{AAS}_m. \tag{29}$$

$$h_m(i,j) = \frac{I^{AAS}_{\boldsymbol{M}}}{3\,(2n-1)\,n_k \sum_{n=1}^{\Psi}\frac{1}{2n-1}}, \tag{30}$$

where $\boldsymbol{M_{S_0}}$ stands for the set of MUEs located at sector 0; n_k is the total number of pixels whose distance d from the center point satisfies $(n-1)\,\psi < d \leq n\psi, d^2 = i^2+j^2$. The calculation of h_n is detailed in Appendix. A. Thus ISM of MUE layer can be constructed in Fig. 4. The ISM of MBS tier changes from sector to sector. Within a sector, if the number of MUEs keep unchanged, the ISM for this sector keeps quite static.

2) Interference State Map Pixel Weight for FBS Layer: In an UDHN, the locations of FBSs actually do not change quite often. However, the activation state of FBSs can vary from time to time. Every FBS has a fixed Voronoi serving area. So the average interference weight $h_f(i,\ j)$ contributed by FBS f to the ISM pixel in the coverage area of FBS f is:

$$h_f(i,j) = \frac{t_f I^{AAS}_f}{n_f}, \tag{31}$$

$$n_f = \frac{S_f}{\psi^2}. \tag{32}$$

t_f is the FBS activation state indicator, i.e. $t_f = 1$ if FBS f is active (FUE exists in the serving area of FBS f), while $t_f = 0$ otherwise. n_f is the total number of pixels in the coverage area of FBS f. S_f is the total coverage area of FBS f. So the ISM of FBS layer can be constructed in Fig.5.

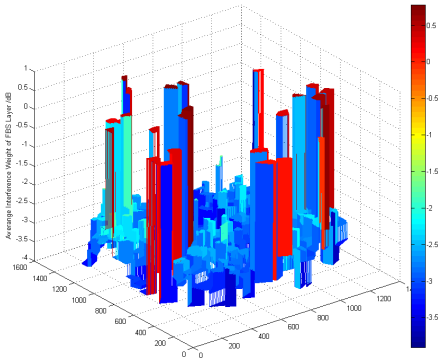

Figure 5. ISM for FBS Layer

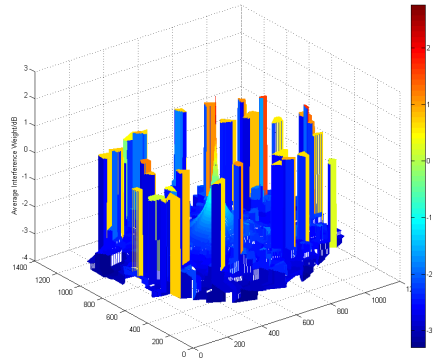

Figure 6. ISM

When the ISM maps from two layers are combined into one, one can get the ISM of the entire network, as shown in Fig. 6.

$$ISM(i,j) = h_m(i,j) + h_f(i,j). \tag{33}$$

C. ISM Similarity Calculation

In the FAS scheme, it is important calculate the similarity among different ISMs in different TSs. Structural Similarity (SSIM) is used to calculate this factor [22], [23]. Assume ISMs at t_0 and t_1 are used to calculate SSIM.

$$\begin{aligned} &SSIM(ISM^{t_0}, ISM^{t_1}) \\ &= SSIM_{(0,1)} \\ &= S_{(0,1)} \\ &= l\left(t_0,t_1\right) \cdot c\left(t_0,t_1\right) \cdot s\left(t_0,t_1\right), \end{aligned} \tag{34}$$

$$l\left(t_0,t_1\right) = \frac{2\mu_{t_0}\mu_{t_1} + C_1}{\mu_{t_0}^2 + \mu_{t_1}^2 + C_1}, \tag{35}$$

$$c\left(t_0,t_1\right) = \frac{2\sigma_{t_0}\sigma_{t_1} + C_2}{\sigma_{t_0}^2 + \sigma_{t_1}^2 + C_2}, \tag{36}$$

$$s\left(t_0,t_1\right) = \frac{\sigma_{t_0 t_1} + C_3}{\sigma_{t_0}\sigma_{t_1} + C_3}, \tag{37}$$

$$\mu_{t_0} = \frac{1}{H*W}\sum_{i=1}^{H}\sum_{j=1}^{W} ISM_{(i,j)}^{t_0}, \tag{38}$$

$$\mu_{t_1} = \frac{1}{H*W}\sum_{i=1}^{H}\sum_{j=1}^{W} ISM_{(i,j)}^{t_1}, \tag{39}$$

$$\sigma_{t_0}^2 = \frac{1}{H*W-1}\sum_{i=1}^{H}\sum_{j=1}^{W}\left(ISM_{(i,j)}^{t_0} - \mu_{t_0}\right)^2, \tag{40}$$

$$\sigma_{t_1}^2 = \frac{1}{H*W-1}\sum_{i=1}^{H}\sum_{j=1}^{W}\left(ISM_{(i,j)}^{t_1} - \mu_{t_1}\right)^2, \tag{41}$$

$$\sigma_{t_0 t_1} = \frac{1}{H*W-1}\sum_{i=1}^{H}\sum_{j=1}^{W}\left(ISM_{(i,j)}^{t_0} - \mu_{t_0}\right)\left(ISM_{(i,j)}^{t_1} - \mu_{t_1}\right), \tag{42}$$

subject to:

$$\begin{cases} C_1 = \left(K_1 \times L\right)^2, \\ C_2 = \left(K_2 \times L\right)^2, \\ C_3 = \frac{C_2}{2}, \\ K_1 = 0.01, \\ k_2 = 0.03, \\ L = ISM_{max}. \end{cases} \tag{43}$$

$ISM_{(i,j)}^{t_0}$ stands for the interference weight of pixel (i,j) in the ISM at t_0; H stands for the height of the ISM, where $H = \Psi$; W stands for the width of the ISM, where $W = 0.866\Psi$; ISM_{max} stands for the biggest interference weight on one pixel. Normally ISM_{max} is attained in the a highly dense situation, where the distance between two nearest MUEs is defined as $d_{min,m}$ and the distance between two nearest FBSs is $R_{min,f}$. Without loss of generality, we assume $d_{min,m} = R_{min,f}$. The calculation of ISM_{max} is in Appendix. B.

D. Cluster-based Sub-band Allocation (CSA) Algorithm

In this part we will construct a fast sub-band allocation algorithm basing on the proposed ISM map by using a cluster-based graph theory model. In this scheme, the interference graph $G(V,E)$ is constructed at MBS. The vertex set V includes all the FBSs and all the MUEs, edge set E stands for the interference relationship between different vertexes. and the MBS makes the allocation

decision. KG is the weight matrix to characterize the potential interference between two vertexes. kg_{ij} and kg_{ij} are different when i and j are in different tiers. When i, j are in the same tier, $kg_{ij} = kg_{ji}$. When $kg_{ij} = 0$, node i and node j are not connected in the graph.

KG is calculated via the following process.

- If both i and j are MUEs, kg_{ij} i given a big value, which means these two UEs are in a strong interference situation. In this situation, these two nodes can not be assigned to one same cluster.
- If i is an MUE and j is an FBS, there exist two scenarios. In scenario 1, MUE i is in the coverage of FBS j. kg_{ij} is set to a big value so that MUE i and FBS j are not assigned to the same cluster. In scenario 2, MUE i is not in the coverage of FBS j. We have $kg_{ij} = \frac{1}{R_{(MU_i, FB_j, A_i)}}$ and $kg_{ji} = \frac{1}{R_{(FB_j, MU_i, A_j)}}$.
- If both i and j are FBSs, we have $kg_{ij} = kg_{ji} = \frac{1}{R_{(FB_i, FB_j, A_j)}}$.

Once the interference graph is constructed, the sub-band allocation problem becomes a graph-based clustering problem, in which users in the same cluster are allowed to share the same sub-band. Assume that the number of sub-bands is $K = |\boldsymbol{K}|$ and the weight between node i and node j is kg_{ij}. In this graph, a node stands for either an FBS or an MUE. A cluster-based sub-band allocation algorithm (CSA) is proposed to control the sub-band allocation process.

The CSA algorithm is constructed based on a labeling mechanism. We divide the CSA algorithm into two stages: labeling stage and sub-band allocation stage.

- Labeling stage
  In this stage, each node is first assigned a pre-label, whose weight is the AAS value of that node.

$$\boldsymbol{L^p} = \{l_i^p | l_i^p = I_i^{AAS}, i \in \boldsymbol{V}\}. \tag{44}$$

- Sub-band allocation stage
  On the condition that the nodes in the same cluster use the same sub-band, the clustering problem becomes a MAX K-CUT problem in the graph theory. How to partition the vertex set $\boldsymbol{V}$ into K disjoint sets $\boldsymbol{D} = \boldsymbol{D_1} \cup \boldsymbol{D_2} \cup ... \cup \boldsymbol{D_K}$ to maximize the weight between the disjoint sets in graph $G = (V, E)$ has been studied. The objective function of the sub-band allocation algorithm can be formulated as:

$$max \sum_{a=1}^{K-1} \sum_{b=a+1}^{K} \sum_{v_i \in \boldsymbol{D_a}, v_j \in \boldsymbol{D_b}} kg_{ij}. \tag{45}$$

  First the algorithm decides whether all the disjoint sets $\boldsymbol{D}$ (from $\boldsymbol{D_1}$ to $\boldsymbol{D_K}$) are empty or not. If all of them are empty, K nodes with the biggest labels are selected as cluster heads, and these K cluster heads are distributed into K sets with each set having one head.

  Then each of the rest nodes are assigned to a cluster. Node v is assigned to a cluster k only when the following conditions are met:

$$\begin{cases} I^{AAS}_{(u, \boldsymbol{D_k} \cup v, A_u)} < \frac{1}{SINR_{th}} & \forall u \in \boldsymbol{D_k}; \\ \Delta KG_k \leq \Delta KG_a & \forall a \in K \\ \Delta KG_k = \sum_{u \in \boldsymbol{D_k}} kg_{vu}; \end{cases} \tag{46}$$

The pseudo-codes of the CSA algorithm are listed in Algorithm 1.

Algorithm 1 CSA algorithms

Initialization: $\boldsymbol{F}$; $\boldsymbol{M}$;$\boldsymbol{K}$; $\boldsymbol{V} = \boldsymbol{F} \cup \boldsymbol{M}$; $KG = [kg_{ij}]_{N \times N}$, $N = |\boldsymbol{V}|$; $N_M = |\boldsymbol{M}|$, $N_F = |\boldsymbol{F}|$; $N_{J_f} = |\boldsymbol{J_f}|$, the number of FUEs served by FBS is f; L is the label matrix of every node; Ω_v is the degree of vertex v; $\boldsymbol{D_k}$ is the set of nodes in cluster k.

function LABEL PROCESS
  Label every node v with l_v, where $l_v = I_v^S$.
end function
function CLUSTER PROCESS
  From $L \downarrow$; $\forall v \in \boldsymbol{V}, k \in \boldsymbol{K}$;
  if cluster k is empty **then**
    $v \rightarrow \boldsymbol{D_k}$;
  else
    Calculate $\Delta KG_k = \sum_{u \in \boldsymbol{D_k}} kg_{vu}$; $I^P_{(u, \boldsymbol{D_k} \cup v)}, \forall u \in \boldsymbol{D_k}$;
  end if
  if $I^P_{(u, \boldsymbol{D_k} \cup v)} < \frac{1}{SINR_{th}}, \forall u \in \boldsymbol{D_k}$&& $k = \arg\min \Delta KG$ **then**
    $v \rightarrow \boldsymbol{D_k}$;
  else
    block cluster k; repeat **if**;
  end if
end function

E. Fast Sub-band Allocation (FSA) Scheme

In the FAS scheme, we assume the MBS will do all the resource allocation decisions and the MBS will store all the allocation results. At each time instant, the FAS scheme consists of three steps:

1) Step 1: ISM construction: In this step the MBS first constructs the current ISM, defined as ISM^1, of the entire network, according to the method in subsection.B. The ISM constructed in the previous time instant is defined as ISM^0.

2) Step 2: ISM matching: If $ISM^0 = \emptyset$, end this step and go to step 3. Otherwise calculate SSIM $S_{(0,1)}$ of ISM^1 and ISM^0. Compare the SSIM value with the ISM Similarity Factor threshold S_{th}.

- If $S_{(0,1)} \geq S_{th}$, $\boldsymbol{D_0}$ is updated to $\boldsymbol{D}$ by keeping static UEs in $\boldsymbol{D_0}$ and remove dynamic UEs from $\boldsymbol{D_0}$.
- If $S_{(0,1)} < S_{th}$, $\boldsymbol{D}$ is set to empty.

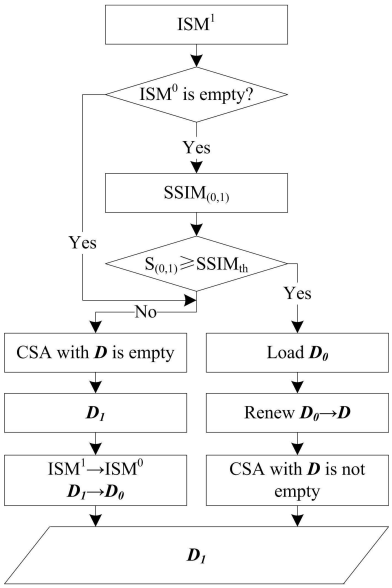

Figure 7. FAS Scheme Flowchart

3) Step 3: sub-band allocation: MBS assigns each UE to a cluster according to the CSA algorithm and cluster set $\boldsymbol{D_1}$ is formed. The corresponding variables are updated in the following.

- If $S_{(0,1)} \geq S_{th}$, both $\boldsymbol{D_0}$ and $\boldsymbol{ISM^0}$ remain unchanged.
- If $S_{(0,1)} < S_{th}$, update $\boldsymbol{D_0}$ and $\boldsymbol{ISM^0}$ with $\boldsymbol{D_1}$ and $\boldsymbol{ISM^1}$ respectively.

The corresponding algorithm flowchart of FAS scheme is presented in Fig.7.

The computational complexity of this scheme comes from three parts. The first part comes from the potential interference estimation, which has a computation complexity $O((N^D)^2)$, $N^D = |\boldsymbol{U_M^D} \cup \boldsymbol{U_F^D}|$. The second part comes from ISM construction, which has a computational complexity $O(\Psi^2)$ and is only a function of the network size. The third part comes from the sub-band allocation, which has a complexity of $O(\frac{(N+N-N^D)(N-N+N^D)}{2}) \approx O((N^D)^2)$. Thus the total computational complexity of the FAS scheme is $O((N^D)^2)$.

IV. Simulation Results

In this section, the performance of the proposed FAS scheme is evaluated via simulation. The simulation parameters are listed in Table 1 by following 3GPP LTE specifications [24].

A 19 cell 57 sector MC configuration is used in the simulation. For a better accuracy on interference evaluation, simulation results are only collected from the central 7 cells [25]. MUEs are randomly distributed over the MC areas and FUEs are randomly distributed in the coverage area of FCs, both following PPP. The path loss model is introduced in Table 2 [26] and the fading follows a Rayleigh distribution. The path-loss from the BS (MBS or FBS) to an UE (MUE or FUE) depends on whether that UE is indoor or outdoor, which is captured by the indicator function. $\delta = 1$ is for indoor and $\delta = 0$ is for outdoor.

Table I
Simulation Parameters

Parameters	Macrocell	Femtocell
System Bandwith	20MHz	20MHz
Subcarrier spacing	180kHz	180kHz
Cell Size	ISD = 500m	Radius = 20m
Cell-center Size	350m	–
Sectors	3	1
Transmit Power	43 dbm	20 dbm
Antenna Gain	14dBi	0dBi
Antenna Type	120°	360°
Antenna back loss	20dB	–
Fast Fading	SCME	SCME
Shadowing Deviation	4 dB	4 dB
Penetration Loss	10dB	10dB
Noise Level	-174dBm/Hz	-174dBm/Hz
UE Distribution Density	$5 * 10^{-4}/m^2$	$1.4 * 10^{-3}/m^2$
Dynamic UE Rate	0.5	0.5

Table II
Path Loss Model

Parameters	Value
MBS to MUE Path Loss	$131.1 + 42.8 * log_{10}\left(\frac{d_{m,B}}{1000}\right) + 20 * \delta_m$
FBS to FUE Path Loss	$127 + 30 * log_{10}\left(\frac{d_{j_f,f}}{1000}\right) + 20 * \left(1 - \delta_{j_f}\right)$
MBS to FUE Path Loss	$131.1 + 42.8 * log_{10}\left(\frac{d_{j_f,B}}{1000}\right) + 20 * \delta_{j_f}$
FBS to MUE Path Loss	$127 + 30 * log_{10}\left(\frac{d_{m,f}}{1000}\right) + 20 * (1 - \delta_m)$

The performance of FAS scheme is compared with three other schemes, namely optimal heterogeneous cluster-based greedy scheme(OHCIG), interference-separation clustering-based scheme (ISC) [17], and multi-cluster based dynamic sub-band assignment (MC-DCA) [15].

Fig. 8 shows the results of optimal S_{th} for the FAS algorithm, where MU stands for all MUEs, FU stands for all FUEs, MMU stands for dynamic MUEs, and MFU stands for dynamic FUEs. As shown in Fig. 8.(a), when the S_{th} increases, the average throughput of MUEs increases slowly and reaches a peak when $S_{th} = 0.6$. The average throughput of MMUs increases simultaneously with the increase of S_{th} and achieves the biggest value when $S_{th} = 0.8$. Further, one can see from Fig. 8.(b) that the average throughput of FUEs can reach two peaks at $S_{th} = 0.6$ and $S_{th} = 0.8$, respectively. Fig. 8.(c) shows the unnecessary sub-band hand-off time (UNHT) of each UE averaged over 100 TSs. As S_{th} increases, UNHT increases sharply and the value is 22.30 when $S_{th} = 0.9$, which means on average a UE can switch its sub-band usage every 4 TSs. By taking the average UE throughput and UNHT into considerations, $S_{th} = 0.6$ is used in the following simulation results.

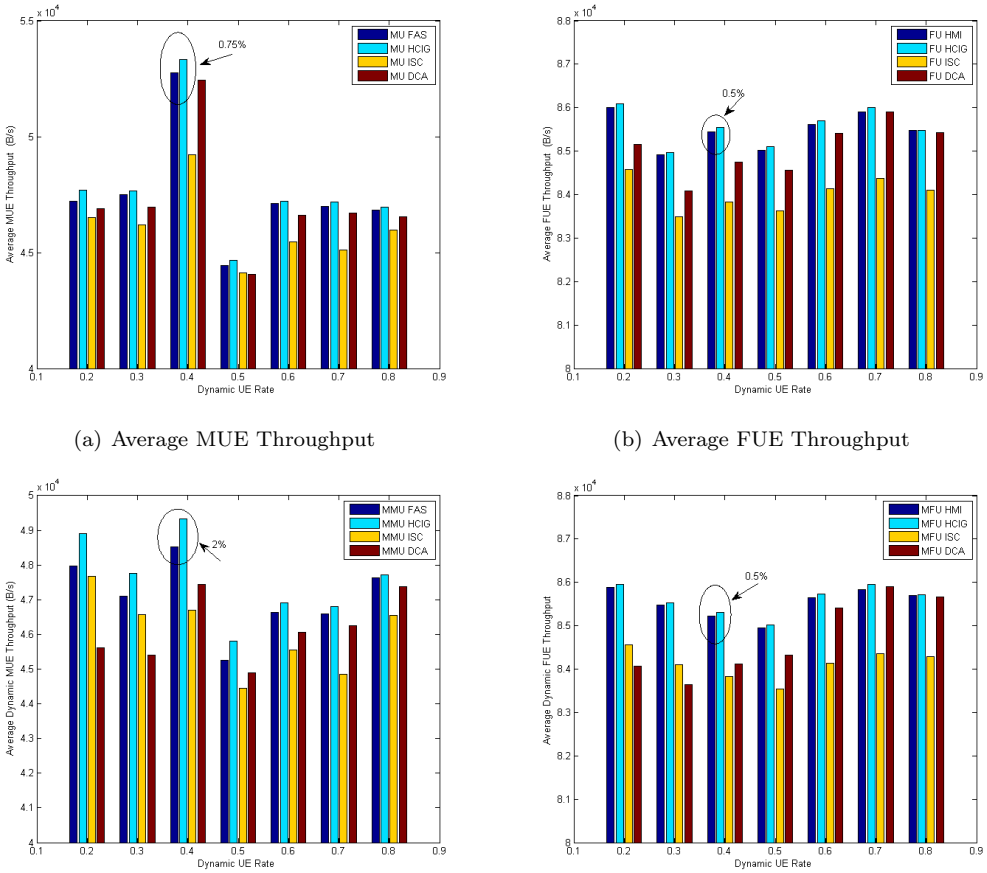

(a) Average MUE Throughput

(b) Average FUE Throughput

(c) Average Dynamic MUE Throughput

(d) Average Dynamic FUE Throughput

Figure 10. Average Throughput of UE with Varying Dynamic UE Rate

Fig.9 shows the average unnecessary sub-band hand-off frequency with different dynamic UE rates. In Fig.10 presents the average throughput of UEs with different dynamic UE rate. In Fig.9, when the dynamic UE rate varies, the performance of FAS scheme is better than the other three schemes. When the dynamic UE rate is 0.4, the average unnecessary sub-band hand-off frequency of FAS is 0.32, which is only the 70% of the OHCIG scheme. And at the same time, as shown in Fig.10(a), the average MUE throughput of FAS scheme is only 0.75% worse than the OHCIG scheme and the average FUE throughput of FAS scheme is only 0.5% worse than HCIG. When it comes to the dynamic UEs, the biggest gap of average UE throughput between the FAS scheme and the OHCIG scheme also appears when the dynamic UE rate is 0.4, which is 2% for MMUE and 0.5% for MFUE respectively.

Fig.11 shows the average unnecessary sub-band hand-off frequency in different MUE density. Fig.12 shows the average throughput of UEs in the different MUE Density. From Fig.11 we can see that, when the MUE density changes, the sub-band hand-off restriction performance of the FAS scheme completely outmatches against the other three schemes. When the MUE density is $6 * 10^{-4}$ per m^2, the sub-band hand-off frequency of FAS scheme is 0.33 per TS, which is 30% better than the OHCIG scheme, 19.5% better than ISC scheme and about 42% better than DCA scheme. While the trade-off of this improvement, as shown in Fig.12, is only 0.2% MUE and 0.23% FUE throughput decrease comparing with the OHCIG scheme. The biggest UE throughput dissimilarity appears at the dynamic MUE throughput. There is an average 1.4% decrease in dynamic MUE throughput comparing with OHCIG scheme. When comparing with the other two schemes, ISC scheme and DCA scheme, the FAS scheme enjoys the comprehensive advantages.

Fig.13 shows the average unnecessary sub-band hand-off frequency in different FUE density. Fig.14 shows the average throughput of UEs in the different FUE Density. From Fig.13 we can see that, when the FUE density increases, the sub-band hand-off restriction performance of all the schemes deteriorates. That is because the more FUEs locate in the measuring area, the more intense communication environment change may happen. That leads to a more frequently sub-band re-allocation. In general, the FAS scheme over performs than the other three schemes. When the FUE density is $1.4 * 10^{-3}$ per

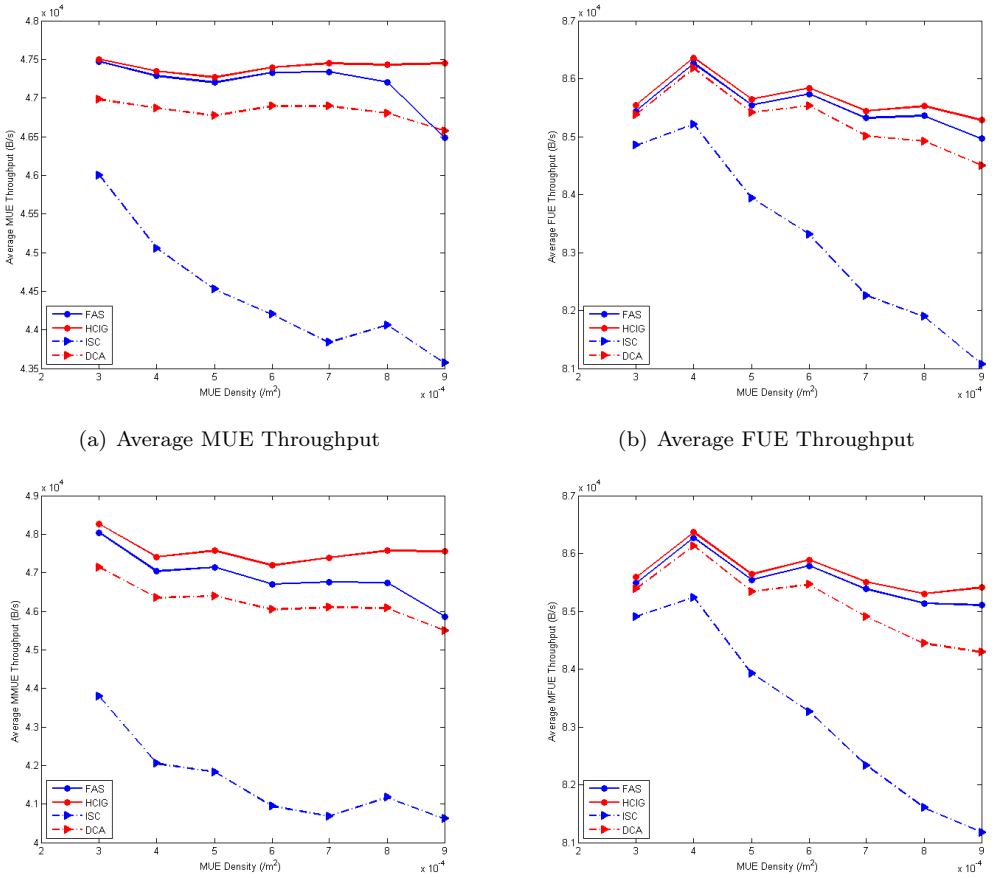

(a) Average MUE Throughput

(b) Average FUE Throughput

(c) Average Dynamic MUE Throughput

(d) Average Dynamic FUE Throughput

Figure 12. Average Throughput of UE with Different MUE Density

m^2, the sub-band hand-off frequency of FAS scheme is 0.325 per TS, while at the same time the OHCIG scheme performs at 0.48. The trade-off of this 32.3% improvement is 3.2% MUE average throughput and 0.7% FUE average throughput degeneration. When comparing with the other two schemes, the FAS scheme has a lower MUE average throughput performance than DCA scheme, while enjoying a comprehensive advantages in other effect parameters.

V. Conclusions

In this paper, a fast sub-band allocation scheme is proposed to mitigate interference in an ultra dense dynamic heterogeneous network via the cluster-based graph theory. In the existing interference mitigation schemes, UEs are normally assigned different sub-bands in different time slots, which leads to a high sub-band hand-off rate and high complexity. In this paper, a new sub-band allocation scheme allows the static UEs to keep their transmit sub-band when the network interference state meets certain conditions. Further, the proposed scheme is more flexible and offers a higher spectral efficiency than other frequency reuse schemes. In this paper, the FAS we proposed with computational complexity $O((N^D)^2)$ has almost the same spectral efficiency compared with the traditional UFR scheme, whose computational complexity is $O(N^2)$. The system level simulation proved that the FAS has a more competitive performance in sub-band hand-off rate and transmit latency and only a little trade-off in user transmit throughput than the other comparing schemes.

Appendix. A

For the calculation of $h_m(i,j)$:

$$\begin{aligned} I_{\boldsymbol{M}}^{AAS} =& \frac{3\omega}{\pi\psi^2} + \frac{3\omega}{\pi\left((2\psi)^2-(\psi)^2\right)} + \\ & \ldots + \frac{3\omega}{\pi\left(\left(n\psi\right)^2-\left(n-1\right)\psi\right)^2\Big)} \\ =& \frac{3\omega}{\pi\psi^2}\sum_{n=1}^{\Psi}\frac{1}{2n-1}, \end{aligned} \tag{47}$$

subject to:

$$\begin{cases} n = \lceil \frac{d}{\psi} \rceil, \\ \psi = \frac{2R}{\Psi}. \end{cases}$$

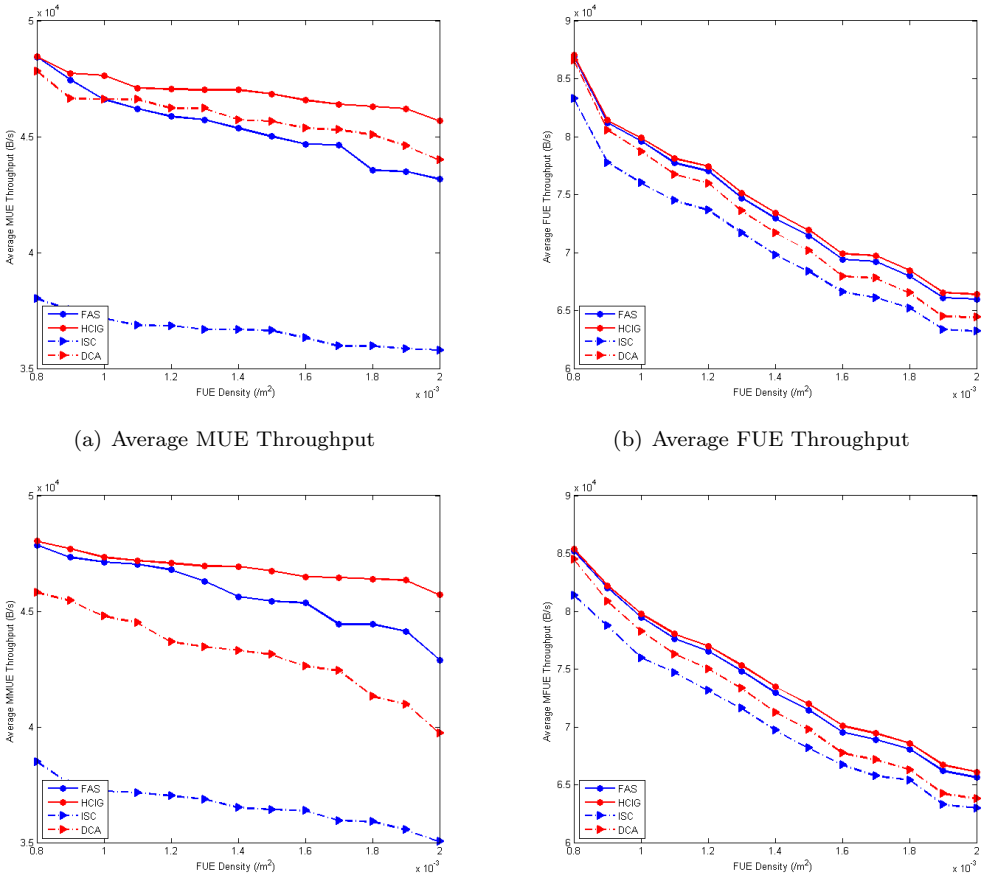

(a) Average MUE Throughput

(b) Average FUE Throughput

(c) Average Dynamic MUE Throughput

(d) Average Dynamic FUE Throughput

Figure 14. Average Throughput of UE with Different FUE Density

We can get:

$$\omega = \frac{\pi\psi^2 I_{\boldsymbol{M}}^{AAS}}{3\sum_{n=1}^{\Psi}\frac{1}{2n-1}}. \tag{48}$$

So:

$$\begin{aligned} h_m(i,j) &= \frac{\omega}{\pi\left(2n-1\right)\psi^2 n_k} \\ &= \frac{\pi\psi^2 I_{\boldsymbol{M}}^{AAS}}{3\pi\left(2n-1\right)\psi^2 n_k\sum_{n=1}^{\Psi}\frac{1}{2n-1}} \\ &= \frac{I_{\boldsymbol{M}}^{AAS}}{3\left(2n-1\right)n_k\sum_{n=1}^{\Psi}\frac{1}{2n-1}}. \end{aligned} \tag{49}$$

Where n_k is the total number of pixels whose distance d with the center point meets $(n-1)\,\psi < d \leq n\psi$.

Appendix.B

According to (19), we can get the limiting value of I_f^{AAS} when FBS f locates overlap with the MBS.

$$\begin{aligned} I_{f,max}^{AAS} &= \sum_{f^*\in\boldsymbol{F^*}}\frac{1}{1+2d_{f^*,f}^2\psi_{f^*}} + \sum_{m\in\boldsymbol{M}}\frac{P_f {d_{m,B}}^2}{P_B {d_{m,f}}^2}. \\ &\approx \frac{N_F-1}{1+2(\bar{d_{f^*,f}})^2\psi_{f^*}} + \frac{N_M P_f}{P_B}, \end{aligned} \tag{50}$$

$$N_F = |\boldsymbol{F}|, \tag{51}$$

$$N_M = |\boldsymbol{M}|. \tag{52}$$

$$\bar{d_{f^*,f}} = \frac{R_{min,f}\sum_{n_1=1}^{N_1}\sum_{n_2=1}^{N_2}\sqrt{\left(0.866n_2\right)^2+\left(n_1-1+0.5n_2\right)^2}}{N_F} \tag{53}$$

Subject to:

$$N_1 = \lceil\frac{R_\Delta}{R_{min,f}}\rceil, \tag{54}$$

$$\frac{N_2}{2} = \begin{cases} min\left(2n_1, \lceil\frac{R'}{R_{min,f}}\rceil\right); & n_1 \leq \frac{R}{2R_{min,f}}, \\ min\left(-2n_1+4\lceil\frac{R}{2R_{min,f}}\rceil, \lceil\frac{R'}{R_{min,f}}\rceil\right); & n_1 > \frac{R}{2R_{min,f}}, \end{cases} \tag{55}$$

$$S_{min} = 0.866R_{min,f}^2, \tag{56}$$

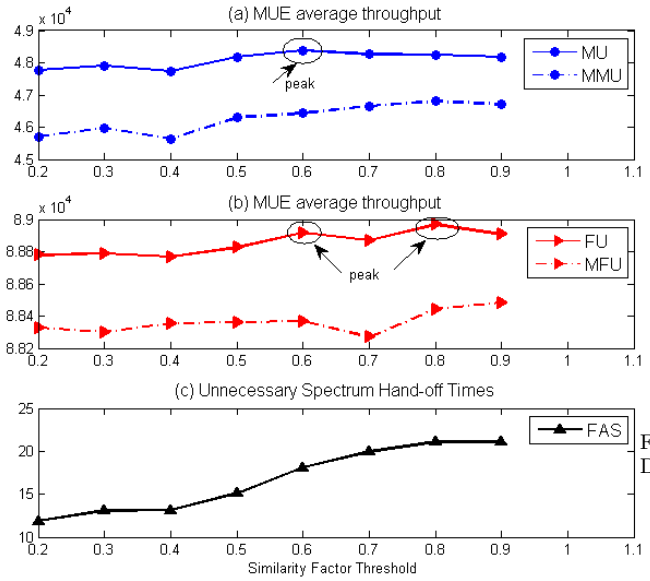

Figure 8. Average UE Throughput and Unnecessary Sub-band Hand-off Time (UNHT) with Different Similarity Factor Threshold S_{th}

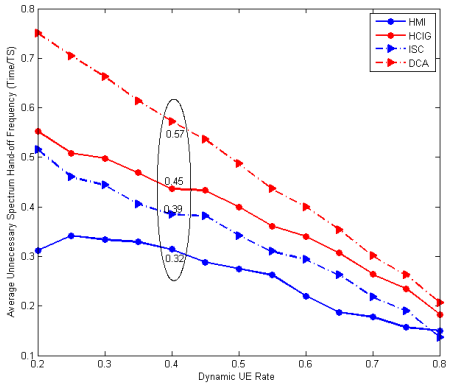

Figure 9. Average Unnecessary Sub-band Hand-off Frequency with Varying Dynamic UE Rate

$$N_F S_{min} = \frac{\pi}{3} R_\Delta^2, \tag{57}$$

$$\frac{2\sqrt{3}}{3}\sqrt{R_\Delta^2 - (n_1 R_{min})^2} = R' \tag{58}$$

Then we can get $h_{f,max}$ like

$$h_{f,max} = \frac{I_{f,max}^{AAS}\psi^2}{S_{min}}. \tag{59}$$

According to (26), we can get the limiting value of I_m^{AAS} when one FBS f locates overlap with MBS.

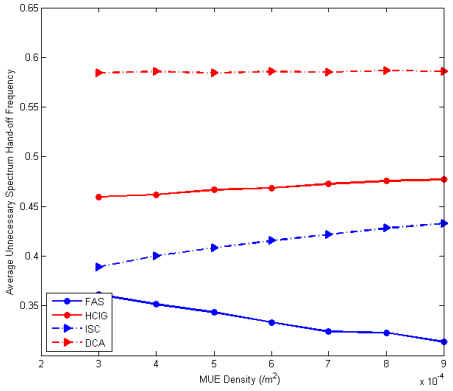

Figure 11. Average Unnecessary Sub-band Hand-off Frequency with Different MUE Density

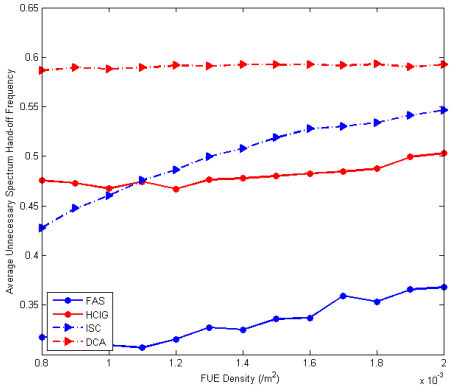

Figure 13. Average Unnecessary Sub-band Hand-off Frequency with Different FUE Density

$$I_{m,max}^{AAS} = \sum_{\substack{m^*,m\in\boldsymbol{M}\\ m^*\neq m}} \lambda_{m^*,m} + \sum_{f\in\boldsymbol{F}} \frac{P_B}{P_f\left(1+2d_{f,B}^2\psi_f\right)} \tag{60}$$

$$\approx N_M - 1 + \frac{N_F P_B}{P_f\left(1+2\bar{d}_{f^*,f}^{\,2}\psi_f\right)} \tag{61}$$

We can get

$$I_{\boldsymbol{M},max}^{AAS} = N_M I_{m,max}^{AAS}. \tag{62}$$

Then, according to (28), we can get $h_{m,max}$ when $n=1$,

$$h_{m,max} = \frac{I_{\boldsymbol{M},max}^{AAS}}{3\sum_{n=1}^{\Psi}\frac{1}{2n-1}}. \tag{63}$$

Then we can get

$$ISM_{max} = h_{f,max} + h_{m,max}. \tag{64}$$

Table III
FREQUENTLY USED NOTATIONS (ORDERED BY APPEARANCE)

Notations	Meaning
R_M	MBS coverage radius
λ_m	MUE density
λ_f	FUE density
R_f	FBS coverage radius
$n_{(m,t)}$	MUE number in TS t
$n_{(f,t)}$	FUE number in TS t
P_{MBS}	MBS transmit power
P_{FBS}	FBS transmit power
k	Sub-band label
m	MUE label
n	MBS (or MC) label
f	FBS label
j_f	FUE j served by FBS f
$P_{B,m}^{k,t}$	Transmit power from MBS to MUE m on sub-band k in time slot t
$h_{B,m}^{k,t}$	Channel gain from MBS to MUE m on sub-band k in time slot t
$G_{B,m}^{k,t}$	Path loss from MBS to MUE m on sub-band k in time slot t
$P_{f,j_f}^{k,t}$	Transmit power from FBS f to FUE j on sub-band k in time slot t
$h_{f,j_f}^{k,t}$	Channel gain from FBS f to FUE j on sub-band k in time slot t
$G_{f,j_f}^{k,t}$	Path loss from FBS f to FUE j on sub-band k in time slot t
$\boldsymbol{M}$	The set of MUEs served by MBS
$s_m^{k,t}$	Sub-band allocation indicator
$\boldsymbol{F^*}$	The set of FBSs covered by MBS except f
$\boldsymbol{J_{f^*}}$	The set of FUEs served by FBS f^*
$\boldsymbol{F^*}$	The set of FBSs covered by MBS
$\boldsymbol{J_f}$	The set of FUEs served by FBS f
$\boldsymbol{K}$	The set of all available sub-bands
N_0	The noise level
$\boldsymbol{U}$	The set of all the UEs in the coverage area of MBS
$\boldsymbol{T}$	The total number of time slot in the whole test stage
$R_{min,f}$	The minimum between FBS and its serving FUE
$d_{f^*,f}$	The distance between FBS f^* and f
$d_{m,f}$	The distance between MUE m and FBS f
$\boldsymbol{\varpi}$	Antenna back loss
$\boldsymbol{\Theta_m}$	Sector label of MUE m
ψ	Pixel length; Minimum distance between two different UEs
$\boldsymbol{M_{S_0}}$	The set of MUEs locate at sector 0
$\boldsymbol{U_M^D}$	The set of dynamic MUEs
$\boldsymbol{U_F^D}$	The set of dynamic FUEs

APPENDIX.C

ACKNOWLEDGEMENTS

This work is supported by National Natural Science Foundation of China (No.51509049), the Heilongjiang Province Natural Science Foundation (No.F201345) and the Fundamental Research Funds for the Central Universities of China (No.HEUCF160812).

REFERENCES

[1] Hwang I, Song B, Soliman SS. A holistic view on hyper-dense heterogeneous and small cell networks. IEEE Commun Mag. 2013;51(6):20-27.

[2] Andrews JG, Buzzi S, Choi W, Hanly SV, Lozano A, Soong AC, Zhang JC. What will 5G be?. IEEE J Sel Areas Commun. 2014;32(6):1065-82.

[3] Peng HA, Xiao Y, Ruyue YN, Yifei YU. Ultra dense network: Challenges, enabling technologies and new trends. China Commun. 2016;13(2):30-40.

[4] Smallcell forum, http://www.smallcellforum.org/

[5] Chen S, Qin F, Hu B, Li X, Chen Z. User-centric ultra-dense networks for 5G: challenges, methodologies, and directions. IEEE Wirel Commun. 2016;23(2):78-85.

[6] Sui Y, Guvenc I, Svensson T. Interference management for moving networks in ultra-dense urban scenarios. EURASIP J Wirel Commun Network. 2015;2015(1):1-32.

[7] Chuang MC, Chen MC, Yeali S. Resource management issues in 5G ultra dense smallcell networks. Proc. IEEE ICOIN;2015;Cambodia.

[8] Mhiri F, Sethom K, Bouallegue R. A survey on interference management techniques in femtocell self-organizing networks. J Network Comput Appl. 2013;36(1):58-65.

[9] Lee YL, Chuah TC, Loo J, Vinel A. Recent advances in radio resource management for heterogeneous LTE/LTE-A networks. IEEE Commun Surv Tutorials. 2014;16(4):2142-80.

[10] Peng M, Wang C, Li J, Xiang H, Lau V. Recent advances in underlay heterogeneous networks: Interference control, resource allocation, and self-organization. IEEE Commun Surv Tutorials. 2015;17(2):700-29.

[11] Abdelnasser A, Hossain E. Subchannel and power allocation schemes for clustered femtocells in two-tier OFDMA hetnets. Proc. IEEE ICC. 2013; Budapest,Hungary.

[12] Anjum O, Yilmaz ON, Wijting C, Uusitalo MA. Traffic-aware resource sharing in ultra-dense small cell networks. Proc. IEEE EuCNC. 2015; Paris, France.

[13] Elsherif AR, Chen WP, Ito A, Ding Z. Adaptive resource allocation for interference management in small cell networks. IEEE Trans Commun. 2015;63(6):2107-25.

[14] Zhou L, Hu X, Ngai EC, Zhao H, Wang S, Wei J, Leung VC. A Dynamic Graph-based Scheduling and Interference Coordination Approach in Heterogeneous Cellular Networks. IEEE Trans Veh Technol. 2016;65(5):3735-48.

[15] Kim SJ, Cho I, Lee B, Bae SH, Cho CH. Multi-Cluster based Dynamic Channel Assignment for Dense Femtocell Networks. KSII Trans Int Inf Syst. 2016;10(4):1535-1554.

[16] Yoon M, Kim MS, Lee C. A Dynamic Cell Clustering Algorithm for Maximization of Coordination Gain in Uplink Coordinated System. IEEE Trans Veh Technol. 2016;65(3):1752-60.

[17] Qiu J, Wu Q, Xu Y, Sun Y, Wu D. Demand-aware resource allocation for ultra-dense small cell networks: an interference-separation clustering-based solution. Trans Emerg Telecommun Technol. 2016;1071-1086.

[18] Zhang Z, Hu RQ, Qian Y, Papathanassiou A, Wu G. D2D communication underlay uplink cellular network with fractional frequency reuse. Proc. IEEE DRCN. 2015;Kansas City,KS,USA.

[19] Gotsis A, Stefanatos S, Alexiou A. UltraDense Networks: The New Wireless Frontier for Enabling 5G Access. IEEE Veh Technol Mag. 2016;11(2):71-8.

[20] Li Y, Niu C, Ye F, Hu RQ. A universal frequency reuse scheme in LTE-A heterogeneous networks. Wirel Commun Mob Comput. 2016;published online.

[21] Tang H, Hong P, Xue K, Peng J. Cluster-based resource allocation for interference mitigation in LTE heterogeneous networks. Proc. IEEE VTC Fall.2012;Quebec City,Canada.

[22] Wang Z, Bovik AC, Sheikh HR, Simoncelli EP. Image quality assessment: from error visibility to structural similarity. IEEE trans image processing. 2004;13(4):600-12.

[23] Hore A, Ziou D. Image quality metrics: PSNR vs. SSIM. Proc. IEEE ICPR. 2010;Istanbul,Turkey.

[24] "Evolved Universal Terrestrial Radio Access (E-UTRA); Radio Frequency (RF) System Scenarios", 3GPP TR 36.942 V8.2.0, Jun. 2010 from www.3gpp.org/ftp/Specs/.

[25] Wei R, Wang Y, Zhang Y. A two-stage cluster-based resource management scheme in ultra-dense networks. IEEE ICCC. 2014; Shanghai,China.

[26] Pantisano F, Bennis M, Saad W, Debbah M, Latva-Aho M. Interference alignment for cooperative femtocell networks: A game-theoretic approach. IEEE Trans Mob Comput. 2013;12(11):2233-46.